Please, cite as: M. Tartuferi, V. D'Alessandro, S. Montelpare, R. Ricci, "Enhancement of savonius wind rotor aerodynamic performance: A computational study of new blade shapes and curtain systems", Energy, 2015, 79(C), pp. 371–384
doi: 10.1016/j.energy.2014.11.023

Enhancement of Savonius wind rotor aerodynamic performance: a computational study of new blade shapes and curtain systems

Mariano Tartuferi [a], Valerio D'Alessandro [a,*], Sergio Montelpare [b], Renato Ricci [a]

[a] *Dipartimento di Ingegneria Industriale e Scienze Matematiche*
Università Politecnica delle Marche
Via Brecce Bianche, 60100 Ancona (AN), Italy

[b] *Dipartimento di Ingegneria e Geologia*
Università degli Studi "G. D'Annunzio" di Chieti-Pescara
Viale Pindaro 42, 65127, Pescara (PE), Italy

Abstract

The Savonius wind turbine appears to be particularly promising for low power applications, such as those in urban areas, and it can take advantage of a simple, reliable and cost-effective construction. Anyway, the Savonius wind turbine suffers from poor performance, when compared with other wind turbines having a major overall complexity and higher costs. For this reason, several studies have been carried-out in recent years in order to improve its energy performance.

The aim of the present work is to enhance the aerodynamic performance of the Savonius wind rotor following two different approaches: the first one is based on the development of innovative airfoil-shaped blades, while the second one concerns the use of a new curtain system, self-orienting relative to the wind direction. For the purpose of the present work has been applied a customized numerical model, previously validated by means of experimental data obtained at the environmental wind tunnel of the Università Politecnica delle Marche.

The obtained results show that both the approaches here proposed, following two distinct guidelines for the development of new and more efficient rotor geometries, are able to produce sensible enhancements in terms of the energy performance of the Savonius wind turbine.

Key words:
Savonius, Vertical axis wind turbine, Computational fluid-dynamics, Wind tunnel testing, Design study.

Nomenclature

C_m	Torque coefficient
$\langle\rangle$	Angular average operator
Re	Reynolds number
C_p	Power coefficient
i	Irregularity degree
$\mathbf{n}$	Outward normal unit vector
$\boldsymbol{\omega}$	angular velocity vector $[\frac{\text{rad}}{sec}]$
$\dot{\boldsymbol{\omega}}$	angular velocity rate vector $[\frac{\text{rad}}{sec^2}]$
λ	Tip–speed ratio
ρ	Fluid density $[kg/m^3]$
θ	Rotor angular position [rad]
$\underline{\underline{\mathbf{T}}}$	Stress tensor $[Pa]$
A	Rotor cross section area $[m^2]$
a_k	Resistant torque coefficients $[Nms^k]$
H_r	Rotor height $[m]$
I	moment of inertia $[kg \cdot m^2]$
L	Domain length $[m]$
P	Extracted power $[W]$
R	Rotor radius $[m]$
u_∞	Incoming wind velocity $[\frac{m}{s}]$
$W_{reference}$	Domain width $[m]$
X	$\mathbf{r}$ vector x–component $[m]$
X'	$\mathbf{r}'$ vector x–component $[m]$
X_0	$\mathbf{r_0}$ vector x–component $[m]$
Y	$\mathbf{r}$ vector y–component $[m]$
Y'	$\mathbf{r}'$ vector y–component $[m]$
Y_0	$\mathbf{r_0}$ vector y–component $[m]$
$\mathbf{M_a}$	Aerodynamic torque $[Nm]$
$\mathbf{M_r}$	Resistant torque $[Nm]$
$\mathbf{M_{ext}}$	Net external torque $[Nm]$
$\mathbf{r}'$	Position vector in the rigid body domain$[m]$
$\mathbf{r_0}$	Position of the rotor center of rotation $[m]$
$\mathbf{r}$	Position vector in the fluid domain $[m]$
$\mathbf{v_{rel}}$	relative wind velocity $[\frac{m}{sec}]$
$\mathbf{v}$	absolute wind velocity $[\frac{m}{sec}]$

* Corresponding author.
Email addresses: m.tartuferi@univpm.it (Mariano Tartuferi), v.dalessandro@univpm.it (Valerio D'Alessandro), s.montelpare@unich.it (Sergio Montelpare), ricci@univpm.it (Renato Ricci).

1 Introduction

The Savonius wind rotor is a small vertical axis wind turbine, created for the first time by the Finnish engineer Sigurd Savonius in 1925. It is commonly classified as a drag driven wind turbine, even if, for some angular positions of the rotor, there may be lift contributions on the torque release mechanism, as evidenced by values of tip speed ratio (λ) greater than one [1].

The Savonius wind turbine is suitable for local electricity production requiring low power, such as street-lighting systems in urban areas [2,3]. For this kind of applications it can take advantage of several aspects: it has a simple, cost-effective and reliable construction; it is well suited to be integrated in urban environment, thanks to the vertical development of its overall design and to low noise emission. In addition, the Savonius wind rotor has no need to be oriented in the wind direction, and it is self-starting due to high static torque values.

Anyway, when compared with other wind turbines, the Savonius rotor exhibits lower performance; for this reason, in the last four decades several authors have tried to develop different solutions, with the common target of resolving its main drawbacks [4]. Such solutions mostly rely on modifying a number of geometrical parameters that affect the performance of the rotor: among these, the number of blades, their relative spacing and overlap, the number of stages and their angular shift, rotor twist angle and aspect ratio; in addition, the use of aerodynamic appendages can be useful to increase rotor global performance.

Nevertheless, a more challenging research area concerns the enhancement of the aerodynamic performance of the Savonius wind rotor by means of the development of new blade shapes. Modi and Fernando [1] proposed a new blades geometry which proved to be able to increase the maximum power coefficient of the rotor ($C_{p,max}$). Rahai et al. [5] realized an aerodynamic optimization process of an airfoil-shaped rotor previously proposed by Benesh [6], getting an enhancement in terms of dynamic behaviour. Kamoji et al. [7] proposed a slightly modified version of the Savonius rotor previously developed by Modi and Fernando [1], gaining improvements in terms of both static and dynamic performance. Mohamed et al. [8], by means of evolutionary algorithms, optimized the blade shape of a Savonius rotor in presence of a flat plate shielding the returning blade: the optimized rotor set-up exhibits considerable enhancements of power output in the entire operating range investigated. Most recently, Kacprzak et al. [9] performed a numerical analysis of conventional and modified Savonius wind rotors, confirming that the use of blade geometries different from the standard semi-cylindrical shape is a promising way to enhance the energy performance of the Savonius rotor; in this effort, numerical investigations play an increasingly central role, as pointed out by Roy et al. [10].

Moreover, another relevant research field concerns the use of suitable aerodynamic devices able to enhance the overall performance of the Savonius wind rotor, by means of the improvement of the flow conditions near the rotor blades. In the last years, several authors [11,12,13,14] proposed many rotor arrangements which proved to be able to achieve higher energy performance, both in static and dynamic conditions, by means of guide-box tunnel, obstacles shielding the returning blade and curtain systems. Depending of the particular design adopted, such aerodynamic devices reduce the negative torque acting on the returning blade and/or increase local wind speed near the advancing blade, channelling the flow towards the rotor in a better manner.

The present work deals with two aspects still not treated into the two main research areas aforementioned: the first one concerns the development of airfoil-shaped blades with variable thickness distribution, while the second one is relative to the design of curtain systems able to self-align with the direction of incoming wind.

Thus, in order to enhance the aerodynamic performance of the Savonius wind rotor, two main guidelines have been followed in this work. The first one consists in identifying innovative designs for rotor blades, based on new airfoil–shaped geometries; the second one concerns the use of a new conveyor–deflector curtain system on the conventional rotor, self-orienting relative to the wind direction.

In this framework, two innovative blade designs for the Savonius wind rotor are presented: they are based on the development of new high cambered airfoil sections, specifically conceived for realizing non conventional blade shapes. The first blade design is based on a reshaping of the original geometry of the Goettingen 462 airfoil, while the second one has been obtained developing a completely new airfoil section.

Due to the complex flow field around a Savonius wind rotor, there are not yet analytical models able to perform a reliable prediction of the aerodynamics of the rotor [15,16]. For this reason, in order to assess the energy performance of the Savonius wind rotor with the above mentioned new blade shapes, it has been used a customized computational model [17,18], previously validated by comparing its results with experimental data obtained at environmental wind tunnel of the Università Politecnica delle Marche. This model is based on coupling the Computational Fluid–Dynamics (CFD) code FLUENT with a custom Matlab numerical algorithm, for the treatment of the fluid-rotor interaction. This numerical model takes advantage of resolving the angular velocity of the rotor as a time-varying variable, according to the unsteady aerodynamics of the Savonius rotor. This is a key point since performing unsteady simulations by means of coupling fluid–flow equations with the rigid–body ones allows to achieve a proper and reliable reconstruction of the dynamic be-

haviour of the Savonius wind rotor [19]. The same computational model has been also applied to investigate a more complex flow field, such as the case of a Savonius rotor with conventional semi-cylindrical blades, provided with an innovative conveyor-deflector curtain system, self-orienting relative to the wind direction. This analysis has proved useful to clarify why the use of such aerodynamic devices enhances the overall energy performance of a Savonius wind rotor. Lastly being the numerical approach reported in [17,18] originally verified without aerodynamic appendages around the rotor blades, in this work has been also performed its further validation in presence of conveyor–deflector curtain system by means of experimental data.

2 New blade shapes and curtain systems

In this section the new blade shapes and the curtain system addressed in this work are presented and their main features are outlined.

2.1 Designing new high-cambered airfoil sections

In order to define innovative blade geometries for the Savonius–type wind rotor, has been adopted, as main guideline, the use of high cambered airfoil sections, with Camber values suitable for replacing conventional semi-cylindrical blade shapes. For this aim a suite of airfoils was developed but for the sake of compactness only the two more effective blade shapes are reported in this paper and deeply analyzed. The first blade geometry has been obtained modifying the Goettingen 462 airfoil (Fig. 17(a)), after a careful inspection of different airfoil sections, selected into the University of Illinois at Urbana-Champaign (UIUC) Applied Aerodynamics Group database [20], according to a preliminary criterion of having Camber values greater than 5% of the chord line. The strategy followed for transforming the shape of the Goettingen 462 airfoil consisted in identifying a suitable increase of the section curvature, in order to induce low pressure regions behind the advancing blade able to produce favourable contributions to the rotor rotation. Thus, the original geometry of the Goettingen 462 airfoil has been reshaped increasing its Camber above 30% of the chord line, paying particular attention to the suction side curvature and to the leading edge radius. This new airfoil section is characterized by a 33% Camber value placed at 45% of the chord line: thus, it has been named *SR3345 airfoil* (Fig. 17(b)), and the corresponding rotor configuration is coded in the following as *SR3345 rotor* (Fig. 2(a)). Our design strategy for the *SR3345* airfoil was obviously aimed at the optimization of the corresponding rotor performance. Thus the Camber was moved, as more as possible, towards the rotors tip in order to increase the torque contribution,

in certain angular positions, of low pressure zones of the airfoil suction side. On the other hand the maximum Camber values was increased in order to enhance the magnitude the suction peak. However in this case an upper limit was prescribed by the strong adverse pressure gradients induced after the suction peak. Finally, in our opinion, a good comprimise has been found in the Camber values here reported.
The second rotor type here introduced has been designed starting from the development of a completely new airfoil geometry, and following the general principle aforementioned of making the rotor blades highly curved. This second airfoil section has been named *SR5050 airfoil* (Fig. 1(c)), having a 50% Camber value placed at 50% of the chord line, and it has been obtained superimposing the thickness distribution of the NACA 0012 airfoil over a mean Camber line of suitable shape. The corresponding rotor configuration is coded *SR5050 rotor* (Fig. 2(b)). It is important to put in evidence that in this rotor section has been adopted a Camber line equal to the classical Savonius rotor. An aerodynamic shaped thickness distribution has been superimposed to the standard Camber line with the aim of using its benefits related to the limitation of flow separations and to increase the magnitude of the suction peak.

2.2 New conveyor-deflector curtain system

As introduced in section 1 an innovative conveyor-deflector curtain system (Fig. 3) has been also developed by means of experimental tests at the environmental wind tunnel of the Università Politecnica delle Marche. Such curtain system is composed of two aerodynamic appendages, partially enclosing the Savonius rotor. The first one, the conveyor, is placed alongside of the advancing blade, with the main target of channelling the incoming wind towards the rotor. The second one, the deflector, is adjacent to the returning blade, and carries out the function of reducing the dynamic pressure acting on it, caused by its motion against the incoming flow.
The curtain system here proposed is able to self–align relative to the direction of the incoming wind: this attitude comes from the particular shape of such device, and it has been experimentally verified at environmental wind tunnel of the Università Politecnica delle Marche. The system has been developed coupling the different aerodynamic appendages, in such a way the resultant aerodynamic torque acting on them is zero. Under the action of the incoming wind, the conveyor exhibits a counter–clockwise torque, while the deflector shows a clockwise torque (see Fig. 3 for a schematic representation). This characteristic behaviour comes from the suitable shapes used for the conveying and the deflecting appendages: indeed, each of them is composed of two distinct elements joined by a hinge, making it possible to adapt their relative position in order to modify the aerodynamic torque acting on the appendage.

A set of wind tunnel tests has been conducted in order to idenfity the proper relative positioning of the four elements constituting the aerodynamic appendages. The obtained shape of the curtain system makes it self-orienting relative to the wind direction. Moreover this attitude has been experimentally verified by means of wind tunnel tests for an incoming wind velocity ranging from 4 to 12 m/s.
A paper with a more in–depth analysis of the experimental tests performed on the curtain system here described is under preparation.

3 Numerical model description

A key point to obtain a reliable reconstruction of the energy performance of the Savonius wind rotor consists in a proper modelling of the rotor rotation. For this reason in this work we exploit an approach, based on the Sliding Mesh Model (SMM), which allows an accurate prediction of the unsteady interactions between the rotor blades and the incoming wind [17]. The main features of our numerical approach are summarized in the following subsections.

3.1 The computational domain

In [17] was verified that, on untwisted classical Savonius rotors, the end plates limit the three–dimensional flow behaviour around the model tips. This element allows to compare experimental results obtained on 3D models to numerical data computed on a 2D domain. For this reason the rotors sections here studied have been modeled with a 2D domain requiring a limited computational load.
Moreover in our numerical approach the fluid domain is composed of two distinct sub-regions. The first one, D_1, contains the wind rotor and in particular it is a moving domain rigidly rotating around a fixed axis normal to the represented plane and passing for the center of the rotor having a diameter of 0.4 m. The second sub-region, D_2, models the remaining portion of the wind tunnel test chamber, and it is fixed in an absolute frame of reference; in particular we have fixed $L = 5.5\ m$ and $W_{reference} = 1.8\ m$. The ratio $2R/W_{reference}$ has been set as in [17] in order to obtain a low solid blockage factor ensuring the possibility to neglect the effect of the lateral walls. On the other hand we have adopted an high value of $L/2R$, *i.e.* 13.75, with the aim to move away to the near–field conditions in the wake region. Inside D_1 domain has been adopted an unstructured triangular mesh, with a boundary layer grid refinement in the near wall region (Fig. 5). D_2 domain has been discretized by means of a structured multi-block mesh.

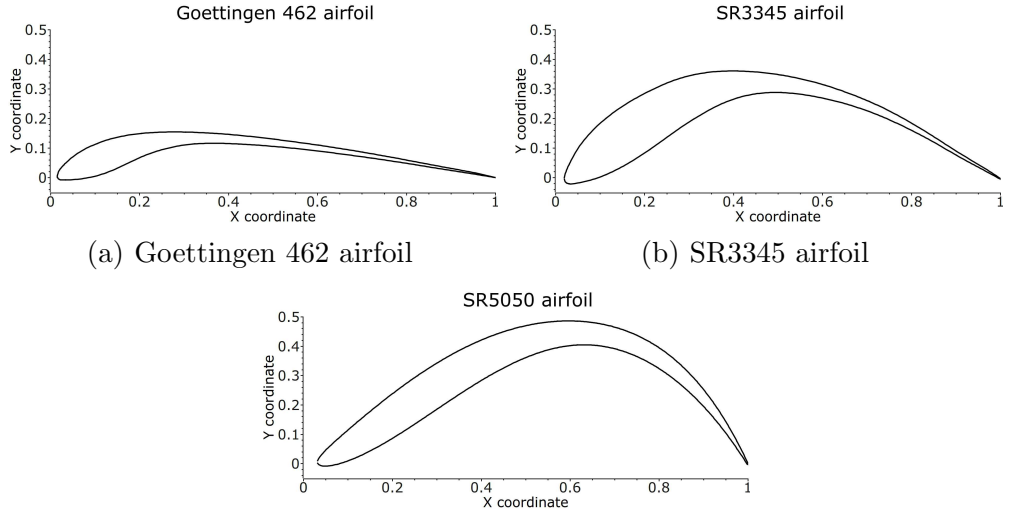

(a) Goettingen 462 airfoil (b) SR3345 airfoil

(c) SR5050 airfoil

Figure 1. *New airfoil-shaped blade sections*

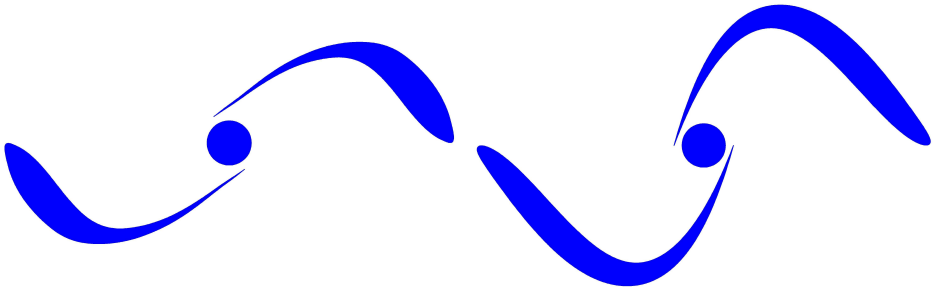

(a) SR3345 rotor (b) SR5050 rotor

Figure 2. *New rotor geometries*

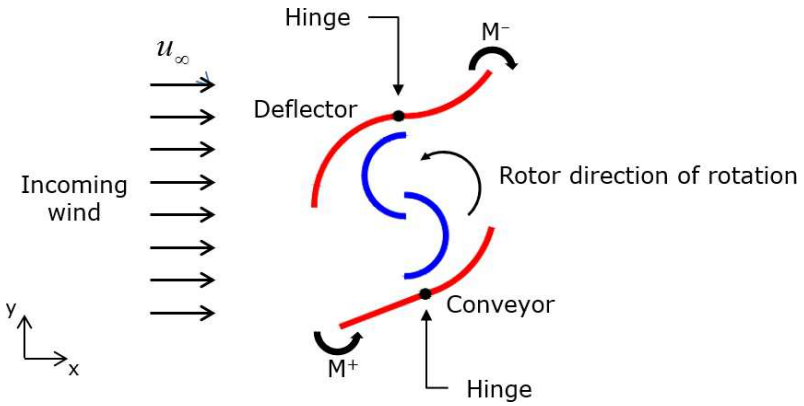

Figure 3. *Sketch of the new conveyor–deflector curtain system, self-orienting relative to the wind direction.*

A slightly different grid arrangement has been used for simulating the flow fields of a Savonius wind rotor, with conventional semi–cylindrical blades, provided with the conveyor–deflector curtain system (Fig. 6). Indeed, the adopted computational domain features for having a three times larger width than that of the fluid domain sketched in Fig. 4; this accounts for strong separations induced by the curtain system, which produces a wider wake than that of the rotor without such aerodynamic appendages: thus, in this manner, the complete wake expansion is guaranteed. Moreover, the conveyor–deflector device has been placed inside a third stationary sub-domain D_3 in such a way its angular position corresponds to the equilibrium position producing self-alignment with the incoming wind; the equilibrium condition of the curtain system has been experimentally verified at environmental wind tunnel of the Università Politecnica delle Marche, and it has been reproduced in the calculations. The same mesh generation strategy previously described has been adopted for D_1 and D_2 sub-domains, discretizing the fluid inside D_3 sub-region by means of a unstructured triangular grid, with boundary layer refinement in the near wall regions.
In all computational grids here employed the viscous sub-layer scaled first centroid distance of the cells next to the walls, y^+, is such that $O\left(y^+\right) \simeq 1$.

3.2 Governing equations and numerical discretization

The flow–fields here studied have been modelled using a two-way coupling between the fluid and the rotor–blades. In particular the solid body motion has been treated solving the second cardinal equation of dynamics by means of a MatLab code able to import CFD data, calculate the rotor angular velocity and export this variable as input to the CFD code. On the other hand, for the turbulent flow around the rotor, the incompressible Reynolds Averaged Navier-Stokes (RANS) equations coupled with different turbulence models have been used (Fig. 9 reports a flow chart of the adopted algorithm).
Starting from numerical solutions the classical energy performance parameters for wind turbines, *i.e.* power coefficient and the torque coefficient, have been obtained as a function of the tip speed–ratio at each rotor angular position. The power coefficient C_p and the torque coefficient C_m are defined respectively as:

$$C_p = \frac{P}{\frac{1}{2}\rho u_\infty^3 A}, \tag{1}$$

$$C_m = \frac{|\mathbf{M}|}{\frac{1}{2}\rho u_\infty^2 A R}, \tag{2}$$

while the tip–speed ratio is defined as:

$$\lambda = \frac{|\boldsymbol{\omega}|\, R}{u_\infty}. \tag{3}$$

In eq. 1, eq. 2 and eq. 3 P represents the extracted power, $\mathbf{M}$ the net aerodynamic torque acting on the rotor, u_∞ the free–stream wind velocity, $\boldsymbol{\omega}$ the angular velocity vector, R the rotor radius and A the frontal area where $A = 2 \cdot R \cdot H_r$ with H_r the rotor height which is fixed to 1 m in all the cases considered in this work.
The instantaneous power P, appearing in eq. 1, is evaluated as:

$$P = \mathbf{M_a} \cdot \boldsymbol{\omega} \tag{4}$$

where $\mathbf{M_a}$ is the aerodynamic torque computed as follows:

$$\mathbf{M_a} = \oint_{\partial\Omega_s} (\mathbf{r}' - \mathbf{r_0}) \wedge \left(\underline{\underline{\mathbf{T}}} \cdot \mathbf{n}\right) d\Gamma. \tag{5}$$

In eq. 5 $\underline{\underline{\mathbf{T}}}$ is the stress tensor including: pressure, viscous and turbulent components, $\mathbf{n}$ is is the outward normal unit vector and Ω_s is the solid body portion. On the other hand $\mathbf{r}' = X'\hat{\mathbf{i}} + Y'\hat{\mathbf{j}}$ is the position vector identifying a generic point in the rotating solid body while $\mathbf{r_0} = X_0\hat{\mathbf{i}} + Y_0\hat{\mathbf{j}}$ is the rotor center of rotation. Note that the origin of the reference frame is placed in left bottom vertex of the computational domain reported in Fig. 4.
Furthermore the performance parameters, reported in eq. 1, eq. 2 and eq. 3, have been averaged over each complete revolution of the rotor, according to eq. 6, eq. 7 and eq. 8.

$$\langle C_p \rangle = \frac{1}{2\pi} \int_0^{2\pi} C_p(\theta)\, d\theta, \tag{6}$$

$$\langle C_m \rangle = \frac{1}{2\pi} \int_0^{2\pi} C_m(\theta)\, d\theta, \tag{7}$$

$$\langle \lambda \rangle = \frac{1}{2\pi} \int_0^{2\pi} \lambda(\theta)\, d\theta. \tag{8}$$

We have to remark that the rotor mean performance, in a fixed operating point, were evaluated averaging the parameters reported in eq. 6, in eq. 7 and in eq. 8 once the asymptotic behaviour was reached, *i.e.* the aerodynamic torque and the resistant torque are "in equilibrium". This corresponds to the

trend of tip–speed ratio illustrated in *Fig.18* of [17] (reported here for the sake of completeness in Fig. 7).

Particular attention has been also devoted to RANS turbulence model selection for the analysis of the two new rotors. For this aim a sensitivity analysis on the conventional Savonius wind rotor with semi–cylindrical blades has been performed using the experimentally determined $C_{p,max}$ point. In particular we have tested the following closure models: SST k–ω [21], the correlation based transition model of Menter and Langtry [22,23], the one–equation Spalart–Allmaras model [24], the v^2–f version of the k–ϵ [25] and the the RNG k–ϵ [26]. In Fig. 8 the comparison, in terms of mean power–coefficient (eq. 6), is reported showing as SST k–ω model agrees very well with experimental data. Moreover it exhibits similar results respect to more complex turbulence models requiring a lower computational load hence it has used for studying the new rotor configurations. This aspect has been a key element in planning the numerical investigations here reported, due to the availability of standard desktop PCs and the aim of studying the fluid-dynamic behaviour of the new rotor designs in several operating points.

In the case of the conveyor–deflector curtain system equipping a conventional Savonius wind rotor with semi–cylindrical blades, more accurate results have been obtained using the v^2-f turbulence model [25] and the Reynolds Stress Model (RSM) with linear pressure–strain closure [27,28]. Such turbulence models have been required by the nature of the flow–field of the Savonius rotor, featured by the strong Reynolds–stress tensor anistropy induced by the presence of the curtain system.

As already introduced the adopted model reconstructs the unsteady aerodynamics of a vertical axis wind rotor providing, for each time step, the solution of the fluid-dynamic field as a function of the instantaneous angular velocity; the latter has been calculated evaluating the rigid body kinematics, and integrating the second cardinal equation of dynamics for a 1–DOF (Degree of Freedom) rotating system (9):

$$I\dot{\boldsymbol{\omega}} = \sum \mathbf{M_{ext}} \tag{9}$$

which is referred to the fixed rotation axis of the system. Torques acting on the rigid body, $\mathbf{M_{ext}}$, are the aerodynamic and the resistant contributions, indicated respectively as $\mathbf{M_a}$ and $\mathbf{M_r}$. The first one derives from the numerical integration of eq. 5 and it is evaluated per unit length; the second one can be computed by means of a H-order polynomial function of the angular velocity with coefficients a_k:

$$\mathbf{M_r} = \left(\sum_{k=0}^{H} a_k \left| \boldsymbol{\omega} \right|^k \right) \widehat{\mathbf{M_r}}. \tag{10}$$

In the present work the resistant torque has been assumed a linear function of the angular velocity ($H = 1$ and $a_0 = 0$) and $\widehat{\mathbf{M_r}}$ is aligned with the direction normal to the rotor plane. H was fixed to 1 in order to reproduce the experimental conditions used for the study of the classical Savonius rotor section reported in [17] .

This allows to express equation (9) in the form of:

$$I\dot{\omega} = \left| \mathbf{M_a} \right| - \left| \mathbf{M_r} \right|, \tag{11}$$

where I is the moment of inertia of the rotor, and $\dot{\omega}$ is the norm of the angular velocity rate vector.

It is worth noting that in our numerical approach RANS equations coupled with the turbulence model, were solved by means of a second order accurate Finite Volume Method (FVM). The convective fluxes were evaluated using a third–order MUSCL approach [29] while diffusive fluxes were computed with a central difference scheme adopting a Green-Gauss cell based method [29]; lastly pressure–velocity coupling was handled with the SIMPLEC [30] approach. For what concerns time-integration a second order accurate implicit scheme [29] was adopted for fluid–flow equations while eq. 11 was solved using a fourth–order accurate explicit Runge–Kutta scheme as in [17]. Moreover our solution procedure adopts an appropriate choice of time–step size in order to avoid overlapped cells at the sliding boundary and assuring conformal grid in every time–step [17].

4 Results and discussions

In order to obtain a detailed characterization of the overall performance of the new Savonius rotor designs, several operating points for both the *SR3345* rotor and the *SR5050* rotor have been simulated, ranging from low to high λ values; being the incoming wind velocity fixed at 9 m/s, this corresponds to model the flow field of the rotor from low to high rotational speeds. Moreover this imply a Reynolds number, computed on the rotor diameter, of about $\mathrm{Re} = 2.34 \cdot 10^5$.

Completing a numerical investigation of such extent required a strong computational effort. Indeed, each operating point (Tab. 1) has been defined imposing a suitable value of the a coefficient in equation (10), performing data

extraction for evaluating results only after a stable periodic working condition has been reached by the rotor: this corresponds, as already introduced in section 3, to the trend of λ illustrated in *Fig.18* of [17], and implies aerodynamic and resistant torques ($\mathbf{M_a}$ and $\mathbf{M_r}$) in equilibrium state. Values of a are in the range 0.01–0.1, and they have been chosen empirically with the following targets: (i) to cover to wide range of tip–speed ratios, thus a good computation of the performance curves; (ii) to obtain a suitable spacing between successive working points. In particular lower a coefficients, corresponding to low resistant torque $\mathbf{M_r}$, identify operating conditions at high λ; vice versa for the case of higher values of a.

In a similar manner, has been performed the numerical investigation of the flow field of a conventional Savonius wind rotor provided with the conveyor–deflector curtain system: anyway, in this particular case, only the operating point corresponding to $C_{p,max}$ has been analyzed (Tab. 2), with the main target of identifying which fluid flow structures are responsible for the higher energy performance as compared with the case of the rotor without such aerodynamic appendages. The analysis has been limited to only one working condition of the rotor because it implied a much higher computational load respect to the rotors without such aerodynamic appendages (about one month of wall–clock time): thus, due to the availability of standard PCs desktop, it was not feasible to reconstruct the fluid-dynamic fields for several operating points of the system. Similarly to case of the new Savonius rotor designs, the incoming wind velocity has been fixed at 9 m/s obtaining the same Re number of *SR3345* and *SR5050* rotors.

4.1 New Savonius wind rotor designs

4.1.1 The energy performance

Compared to a standard Savonius wind rotor with conventional semi-cylindrical blades, both the new developed rotor designs seem to able to gain some improvements in terms of energy performance (Fig. 10) evaluated in terms of average parameters (eq. 6, eq. 7 and eq. 8). For $\lambda < 0.5$ the *SR3345* rotor shows C_p and C_m values slightly greater than those of the standard Savonius rotor and the *SR5050* rotor. For $0.5 < \lambda < 0.9$ the energy performance of the *SR5050* rotor is similar to that of the conventional rotor, while for $\lambda > 0.9$ the *SR5050* rotor exhibits higher power and torque coefficients compared to the values of the classical wind rotor.

Another aspect worth to be particularly emphasized concerns the overall trend of the power curve in the region of $C_{p,max}$, for both the *SR3345* and *SR5050* rotors. Indeed, as evidenced by Fig. 10(a), the new rotor designs here proposed

SR3345 ROTOR		SR5050 ROTOR	
λ	C_p	λ	C_p
0.36	0.17	0.40	0.16
0.41	0.18	0.50	0.19
0.48	0.20	0.64	0.21
0.56	0.21	0.72	0.22
0.65	0.22	0.85	0.23
0.69	0.21	0.96	0.24
0.78	0.21	1.03	0.25
0.85	0.20	1.13	0.24
0.88	0.20	1.23	0.24
0.94	0.19	1.32	0.23
0.99	0.19	-	-
1.08	0.18	-	-
1.16	0.17	-	-

Table 1
List of simulated operating points for the new Savonius wind rotor designs.

have values of C_p slowly decreasing after the λ value corresponding to the maximum power output; this behaviour makes the power curve rather flat in the area of $C_{p,max}$, with a clear advantage from an operational point of view. For this reason, when compared with the standard Savonius rotor, the *SR3345* and *SR5050* rotors exhibits a major flexibility in terms of coupling with the power generator.

The irregularity degree i has been also evaluated as an additional performance parameter, according to the following definition

$$i = \frac{|\boldsymbol{\omega}|_{max} - |\boldsymbol{\omega}|_{min}}{|\boldsymbol{\omega}|_{mean}} \tag{12}$$

where $|\boldsymbol{\omega}|_{max}$, $|\boldsymbol{\omega}|_{min}$, and $|\boldsymbol{\omega}|_{mean}$ are respectively the maximum, minimum and mean norm values of the rotor angular velocity, during a complete revolution in the aforementioned steady periodic working condition. From this point of view (Fig. 11), for $\lambda > 0.6$ the new rotor designs show similar values and trends as those of the standard Savonius wind rotor, while for low values of λ

the *SR3345* rotor exhibits a considerable degree of irregularity. This particular behaviour might be related to the lower moment of inertia of the *SR3345* rotor as compared with the *SR5050* and the standard Savonius rotors, and to the presence, for some angular position of the rotor, of strong suction regions behind the advancing blade (Fig. 13), that make the local rotational speed much higher than its mean value. However, this is not so much a worrying drawback of the *SR3345* rotor, because it exhibits high values of i at very low λ, while for values of λ in the region of $C_{p,max}$ the irregularity degree has the same magnitude of a conventional Savonius wind rotor. Finally we have to note that the moment of inertia per unit length for the *SR5050* rotor is 0.2926 $\mathrm{kg} \cdot \mathrm{m}^2$ while for *SR3345* is 0.2295 $\mathrm{kg} \cdot \mathrm{m}^2$. In both the cases we have hypothesized as material the polycarbonate.

Analysing the polar plot of the torque coefficients corresponding to maximum power output (Fig. 12), the *SR3345* rotor seems to be able to gain some improvements when compared to the other two rotors. Indeed, the *SR3345* rotor shows positive values of C_m in every angular position of a complete revolution, while the standard Savonius rotor exhibits negative values of the torque coefficient for θ ranging between 300°–330° (0° angular position of the rotor is shown in (Fig. 13). This behaviour is particularly evident for the *SR5050* rotor, whose C_m values enters deeply the shaded region of the polar plot corresponding to negative torque coefficients.
Lastly we have to put in evidence that, within the suite of configurations developed during this research (not fully reported for the sake of compactness), *SR3345* and *SR5050* rotors are the more efficient. However it is our intention to remark that the selection was performed on the basis of the performance parameters, above described, which are particularly relevant for practical applications of wind rotors.

4.1.2 Flow fields analysis

A proper description of the aerodynamic behaviour of the Savonius wind rotor requires the analysis of the fluid flow structures from the point of view of the rotor. This can be made reconstructing the complex flow field developing around the rotor by means of the relative wind velocity, in order to take into account how the rotor blades actually interact with the incoming flow. The relative wind velocity $\mathbf{v_{rel}}$ has been computed according to the general equation

$$\mathbf{v} = \mathbf{v_{rel}} + \langle \boldsymbol{\omega} \rangle \wedge (\mathbf{r} - \mathbf{r_0}) \tag{13}$$

where $\mathbf{v}$ is the absolute wind velocity and $\langle \boldsymbol{\omega} \rangle$ is average the angular velocity vector of the rotor, after a stable period working condition has been achieved; $\mathbf{r} = X\hat{\mathbf{i}} + Y\hat{\mathbf{j}}$ is the position vector identifying a generic point in the fluid

portion of the computational domain. Note that the origin of the reference frame also in this case is placed in left bottom vertex of the computational domain.

The flow–field in the blade region for *SR3345* rotor, during a complete revolution at $C_{p,max}$, has been characterized using pressure contours with streamlines of relative velocity.

When the *SR3345* rotor is normal to the free–stream wind velocity (Fig. 13), two main vortex structures are clearly recognisable on the back of the rotor. Behind the advancing blade there is a vortex core maintaining the flow attached to the blade, and determining a wide region of low pressure which is the main responsible of the torque generation of the advacing blade. Two other vortex cores of different dimension are confined within the concave side of the returning blade, due to the action of the jet flow passing through the gap between the returning blade and the rotor shaft (Fig. 14).

During the rotor rotation the aforementioned vortex structures interact with each other, producing the typical wake developing behind a Savonius wind rotor: this is evident from the turbulence intensity map shown in Fig. 15.

For the sake of completeness, Fig. 16 shows the flow field contour plots for a complete revolution of the *SR5050* rotor at $C_{p,max}$. Similar conclusions as for the *SR3345* rotor hold also for the *SR5050* wind rotor.

4.2 The conveyor–deflector curtain system self-orienting relative to the wind direction

The curtain system here proposed is the only known in the literature able to self-align with the direction of incoming wind [2]. Having experimentally verified this attitude at environmental wind tunnel of the Università Politecnica delle Marche, in the present work the attention has been focused on investigating the complex fluid-dynamic phenomena responsible for the higher energy performance of a conventional Savonius wind rotor with such aerodynamic appendages. Considering the innovative design of the conveyor–deflector device and the lack of available similar studies, a CFD reconstruction of the flow field made it possible to gain an insight on how fluid interactions with rotating and stationary elements of the whole system determines the power output increase.
Lastly we have to remark that the standard Savonius rotor here considered (equipped with the new curtain system) is exactly the same deeply investigated in [2,17,18].

v^2-f TURBULENCE MODEL			
λ		$C_{p,max}$	
Exp.	*Num.*	*Exp.*	*Num.*
0.751	0.729	0.301	0.277
Err. 2.9 %		Err. 8 %	
RSM TURBULENCE MODEL			
λ		$C_{p,max}$	
Exp.	*Num.*	*Exp.*	*Num.*
0.751	0.718	0.301	0.274
Err. 4.4 %		Err. 9 %	

Table 2
Comparison between experimental data and numerical results at $C_{p.max}$ for a conventional Savonius wind rotor with the conveyor–deflector curtain system.

4.2.1 The energy performance

The use of a curtain system like that here proposed produces an overall improvement of the energy performance of a conventional Savonius wind rotor, increasing C_p values over the whole range of working points: this is evident by the inspection of Fig. 17, that shows an enhancement of maximum power output greater than 20% relative to the rotor without aerodynamic appendages. Fig. 17 shows also a performance comparison in terms of torque coefficients.

As previously specified, CFD computations have been performed only for the operating condition corresponding to $C_{p,max}$ (experimentally evaluated); Tab. 2 shows the final values of the mean power coefficient and the related percentage errors as compared to experimental data. Both the v^2-f and RSM turbulence models exhibit a good agreement with the experimental values, being the overall accuracy of the first one slightly higher. Thus, they can be assumed reliable and fully equivalent for the purposes of the investigation to perform.

Even in this case, has been evaluated the irregularity degree of the rotor, obtaining the results shown in Fig. 18. By the inspection of the trends reported, it is clear that the irregularity degree is quite higher; this is particularly evident for the v^2-f turbulence model, and it is substantially confirmed by the RSM approach, even if with slightly lower values of i.

Anyway, even if the use of the conveyor–deflector device here proposed increases the irregularity degree of a Savonius wind rotor, such drawback is largely compensated by the fact that, at the same time, it guarantees a remarkable enhancement in terms of the power output, with the additional advantage of being self-orienting relative to the wind direction. The latter attitude is a fundamental requirement to maximize energy extraction from the incoming wind, when the rotor is provided with a curtain system playing the role of a guiding box vane.

4.2.2 Flow fields analysis

The analysis of the fluid-dynamic field allows to clarify which are the main reasons directly responsible for the higher energy performance of the conventional Savonius wind rotor when provided with the curtain system aforementioned. Two are the standpoints for outlining such kind of investigation: the first one pertains to a global point of view, considering the entire flow field, while the second one is of local type, focusing on characteristic fluid flow phenomena in the near rotor region.

The pressure contour depicted in Fig. 19 allows to appreciate the dimensions of the wake featuring such rotor arrangement. The adoption of the conveyor–deflector curtain system induces a blockage-like effect upstream the rotor, producing two important consequences. The first one consists in the generation of a wider wake than that of the rotor without the aerodynamic appendages: this aspect is particularly evident comparing the width of the wake with that reported in *Fig. 26* of [17], and justifies the need of using the grid arrangement sketched in Fig. 6. The second consequence is relative to the increased pressure drop across the rotor section, that guarantees a greater flow quantity to be elaborated: from a global point of view, this is the main reason explaining the higher energy performance of the Savonius wind rotor equipped with the conveyor–deflector device here described.

A close investigation of the fluid flow structures in the near rotor region (Fig. 20) makes it possible to clarify which local fluid-dynamic phenomena determine the enhancement of the overall performance. The conveyor channels the incoming wind toward the advancing blade in a better manner and, thanks to its extension up to the rear side of the rotor, increases the interaction angle between flow and blade. Moreover, the deflector plays the fundamental role of a shielding appendage, avoiding the drag induced by the dynamic pressure of the incoming flow acting on the returning blade. Thus, the combined effects of such aerodynamic appendages allow the rotor to realize a more efficient energy extraction from the wind, getting a relevant enhancement in terms of the power output of the system.

5 Conclusions

The present work summarizes and collects final results of a wide research activity aimed at enhancing the energy performance of the Savonius wind rotor. By means of a detailed computational study, two different guidelines have been followed in order to get this target: the first one consists in the development of new blade geometries, different from the conventional semicylindrical shape, while the second one is based on the use of an innovative conveyor-deflector curtain system.

Designing new airfoil-shaped blades proved to be a challenging task, as rotor interaction with the incoming flow is strongly dependent on geometric features of the blades. New blade geometries here proposed are both based on the common principle of imposing a considerable increase of the mean Camber line of a base airfoil shape, in order to design a section of suitable curvature for replacing the traditional semicylindrical blade geometry. In this context, two new rotor configurations have been proposed, named *SR3345* and *SR5050* rotors, which both guarantee several enhancements in terms of the energy performance; indeed, both these rotor designs take advantage of low pressure regions behind the advancing blade able to produce favourable contributions to the rotor rotation, and hence to the power output. Thus, the results obtained confirm that the development of airfoil-type blades is a promising way in order to get higher energy performance for the Savonius wind rotor.

Moreover, an innovative conveyor-deflector curtain system has been proposed as an alternative way to obtain similar improvements. The key element of such curtain device is in its attitude to be self-orienting relative to the wind direction: this behaviour has been experimentally verified at environmental wind tunnel of the Università Politecnica delle Marche, and has a crucial role in order to maximise the energy extraction from the incoming wind. By means of the same computational approach used for the development of the new rotor designs, a detailed investigation of the fluid-dynamic field of a conventional Savonius rotor with such aerodynamic appendages has been realized. This analysis clarified that a proper coupling of a conveyor device with a deflector one channels the flow in a better manner toward the advancing blade, while at the same time avoiding the drag induced by the dynamic pressure acting on the returning blade.
The results described in the present reaserch confirm that both the adopted guidelines represent a feasible way to enhance the overall performance of the Savonius wind rotor. Such guidelines correspond to diffent philosophies for the development of more efficient rotor configurations, and they can coexist together. Indeed, the adoption of the conveyor-deflector curtain system is more effective in terms of the power output increase but, at the same time, makes the rotor construction more complex. Conversely, the use of airfoil-shaped blades

guarantees some ehancements of the energy performance as compared with the case of a Savonius wind rotor with semicylindrical blades, while preserving its characteristic simple construction. Therefore, the final choice between the strategies here described is not unique, depending on the particular case to deal with.

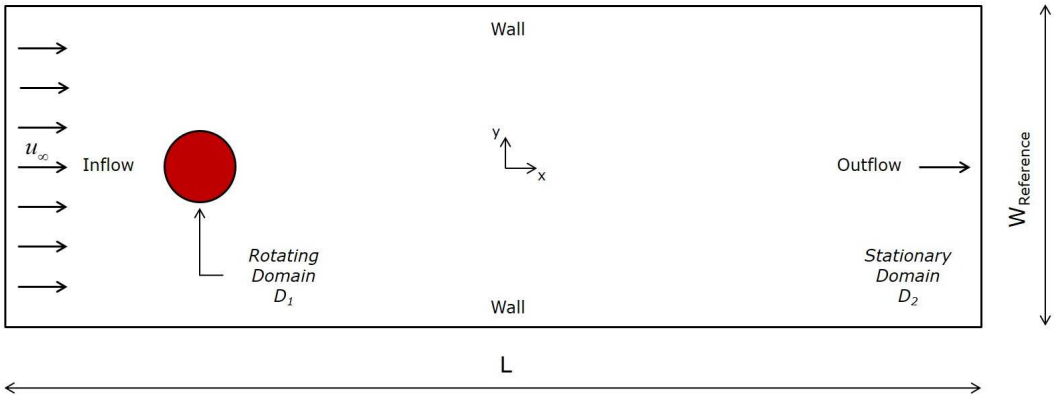

Figure 4. *Layout of the computational 2D domain reproducing the test chamber of the environmental wind tunnel of the Università Politecnica delle Marche.*

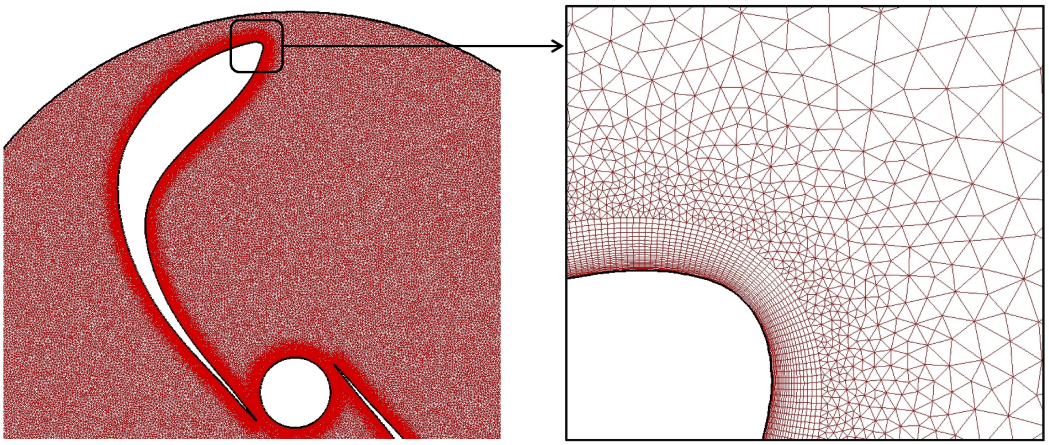

Figure 5. *Details of the grid arrangement inside D_1 domain for the SR3345 rotor: mesh region near the rotor blades (left), and grid refinement near the blade tip (right).*

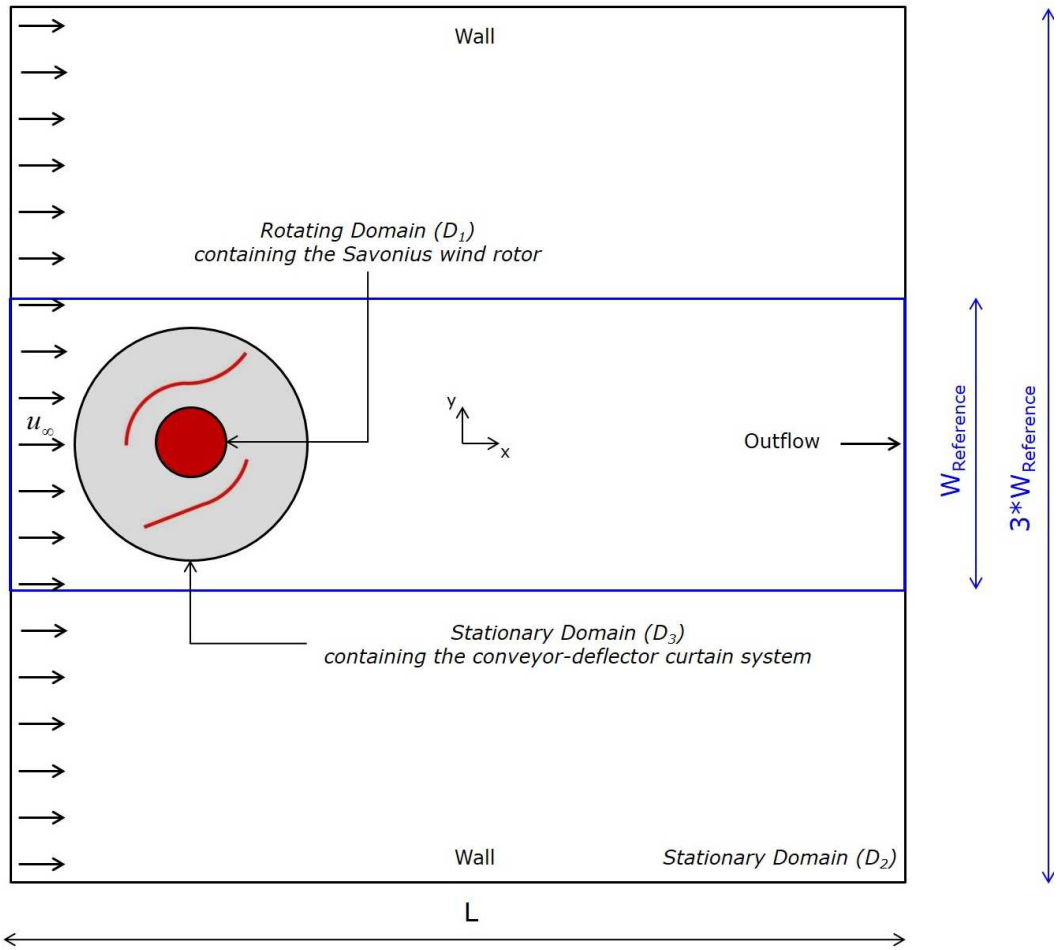

Figure 6. *Layout of the computational 2D domain for a conventional Savonius wind rotor, with semi–cylindrical blades, provided with the conveyor–deflector curtain system.* $W_{Reference}$ *is the reference width of the computational domain showed in Fig. 4.*

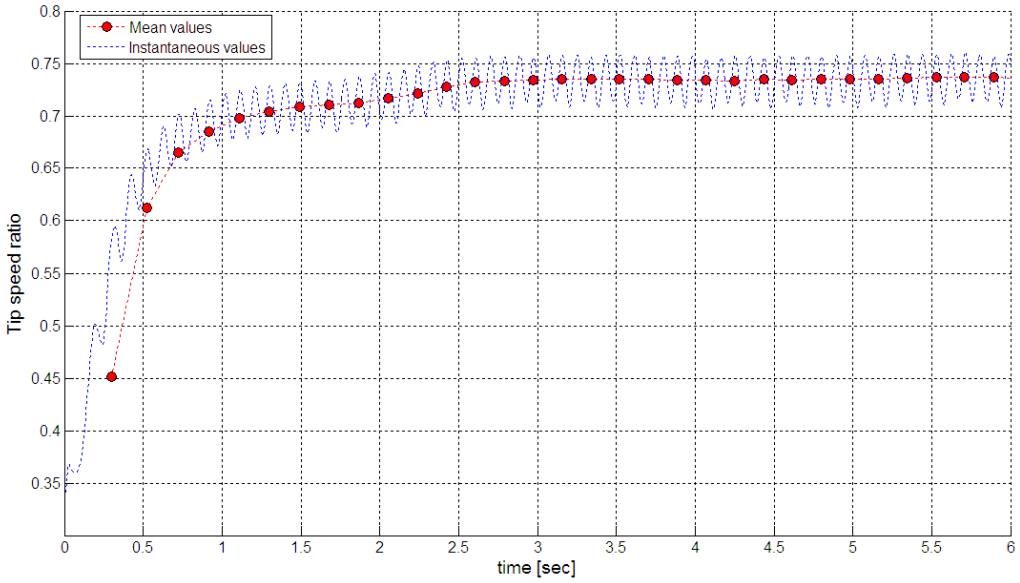

Figure 7. *Classical Savonius wind rotor. Mean tip–speed ratio versus rotation number (Experimental value: $\lambda = 0.735$),[17].*

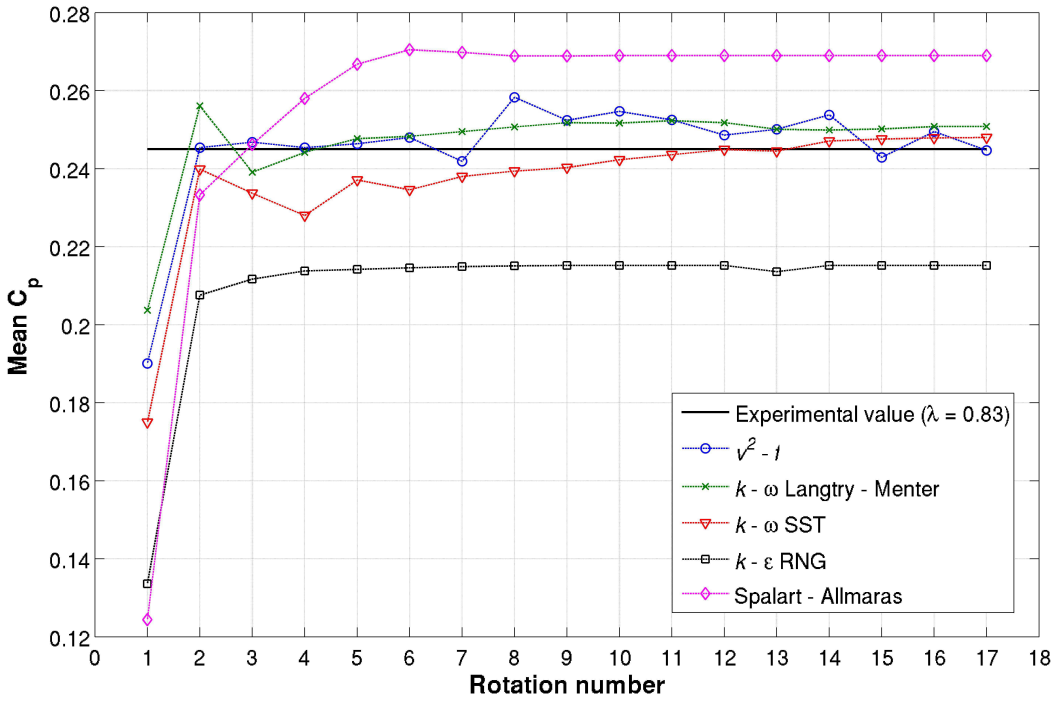

Figure 8. *Turbulence models comparison for a conventional Savonius wind rotor with semi–cylindrical blades.*

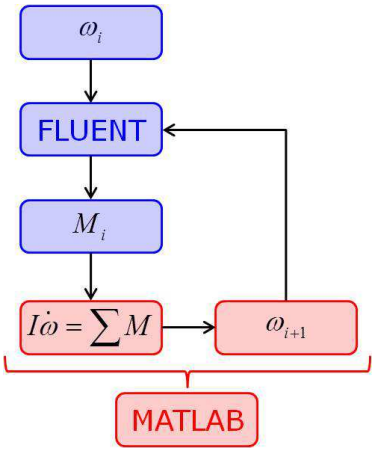

Figure 9. *Flow chart of fluid-rigid body coupling algorithm.*

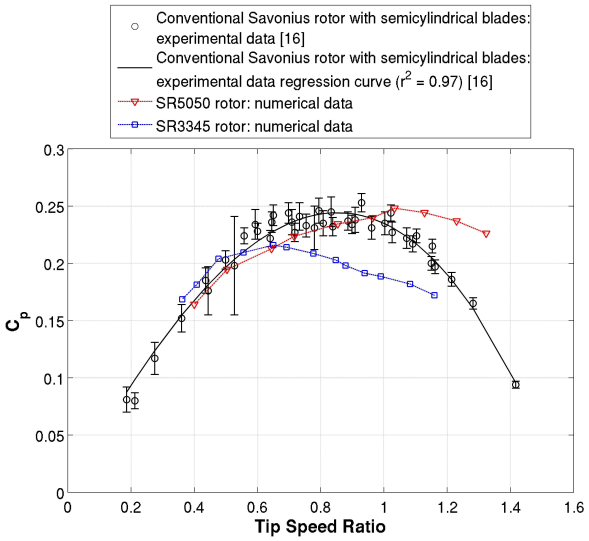

(a) Power curve

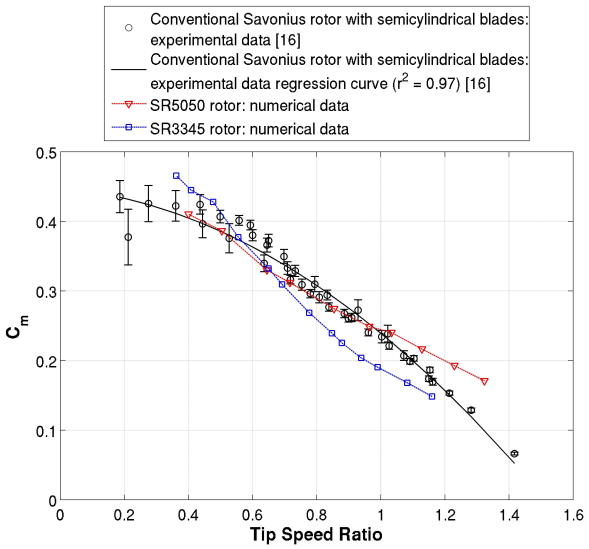

(b) Torque curve

Figure 10. *Performance curves comparison.*

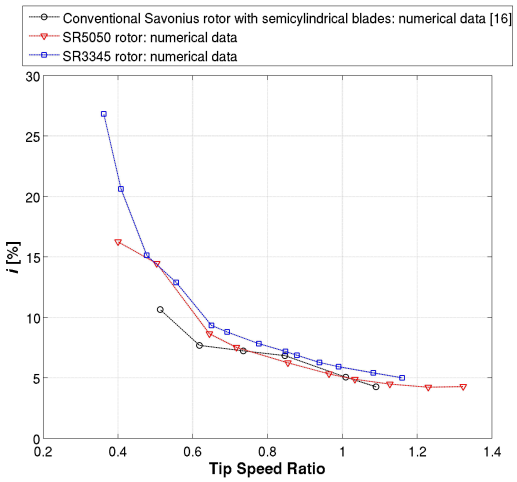

Figure 11. *Irregularity degree comparison.*

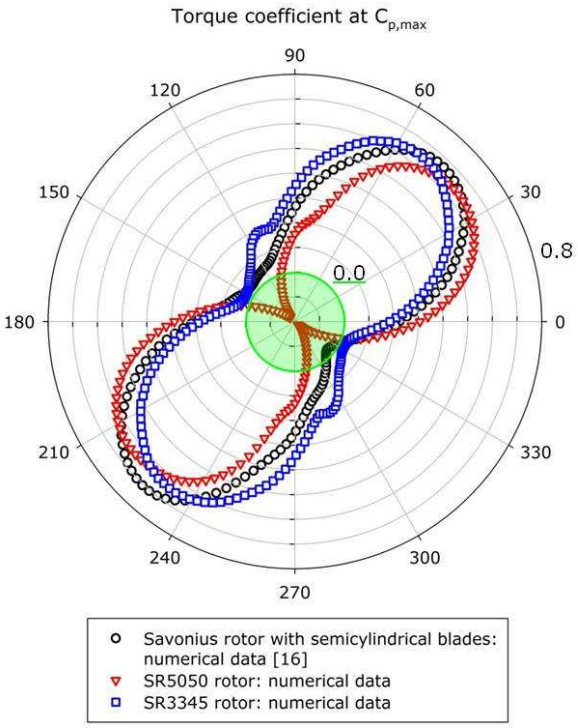

Figure 12. *Torque release comparison.*

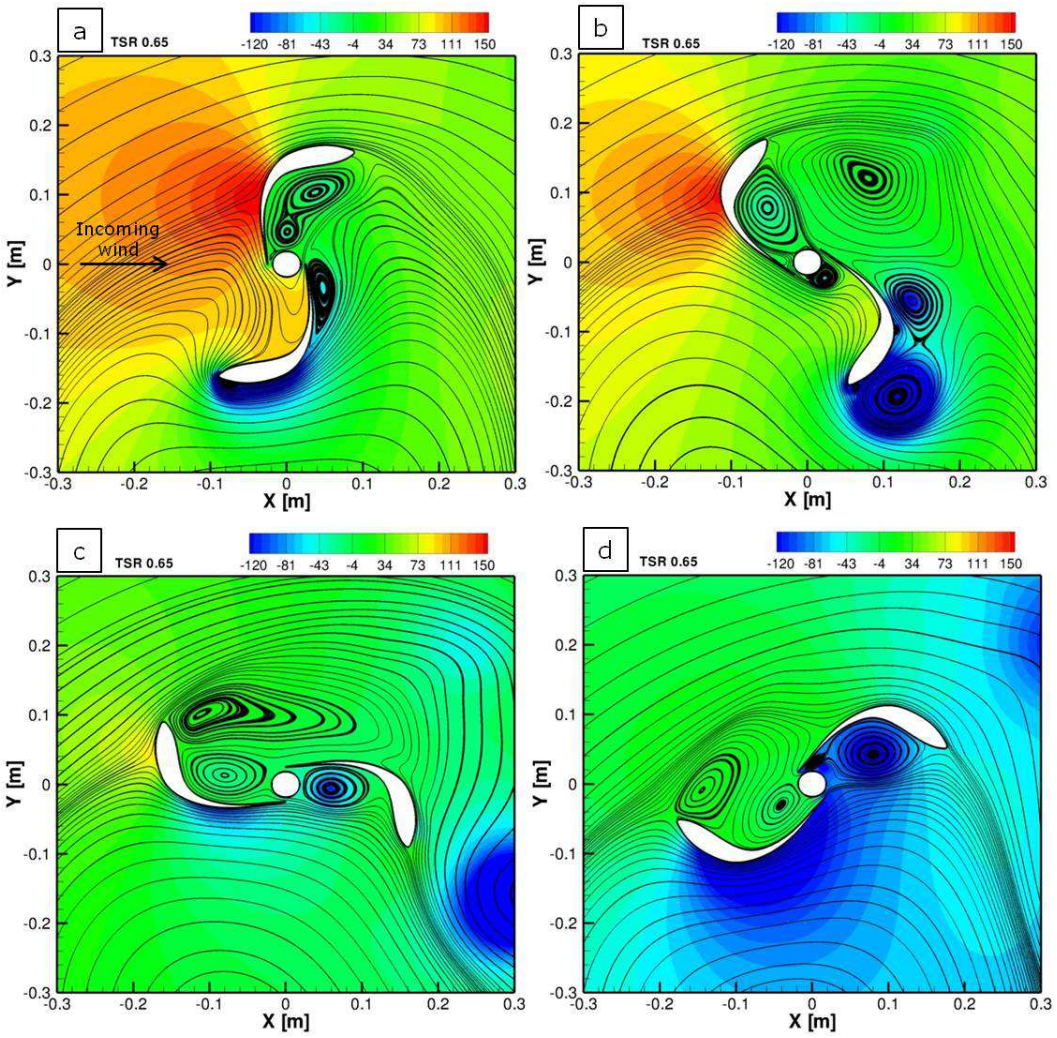

Figure 13. *Contour of static pressure [Pa] for the SR3345 rotor during a complete revolution at* $C_{p,max}$ *(*$\lambda = 0.65$*). (Counterclockwise rotor rotation).*

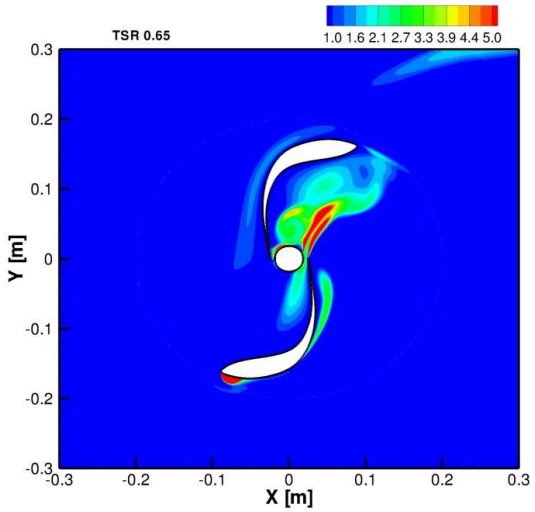

Figure 14. *Contour of turbulent kinetic energy* $[m^2/s^2]$ *for the SR3345 rotor at* $C_{p,max}$ *(*$\lambda = 0.65$*).*

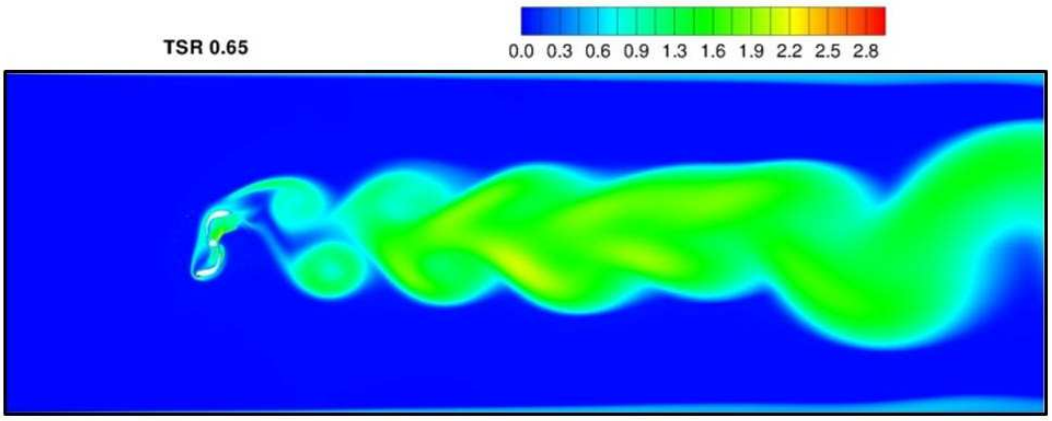

Figure 15. *Contour of turbulence intensity for the SR3345 rotor at* $C_{p,max}$ *(*$\lambda = 0.65$*).*

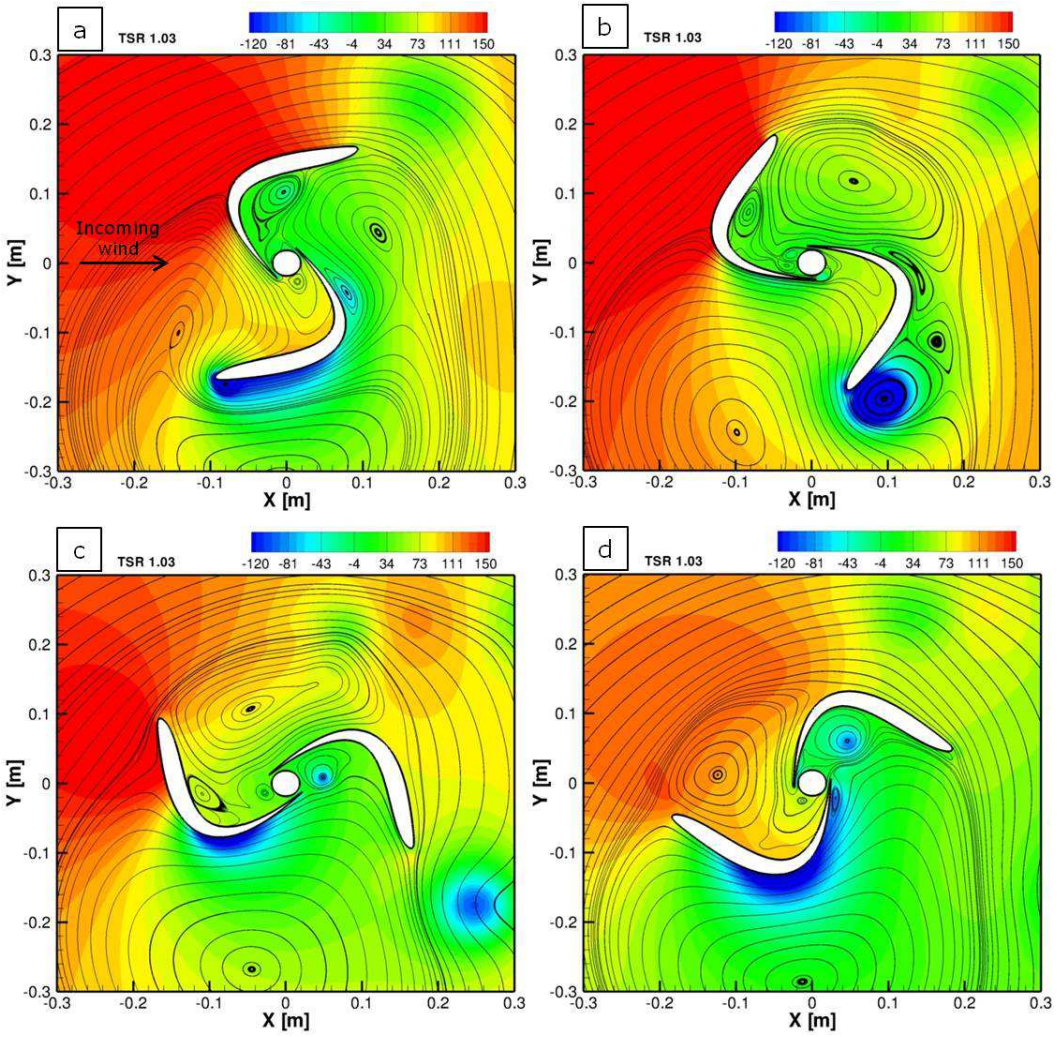

Figure 16. *Contour of static pressure [Pa] for the SR5050 rotor during a complete revolution at* $C_{p,max}$ *(*$\lambda = 1.03$*). (Counterclockwise rotor rotation).*

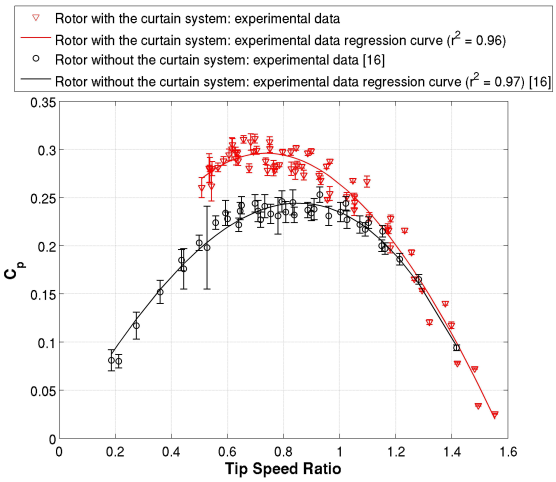

(a) Power curve

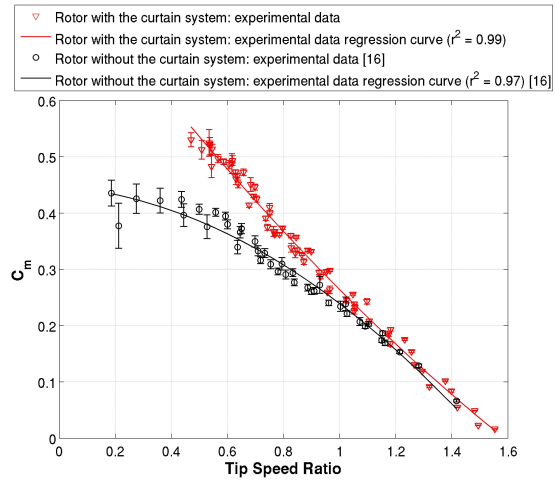

(b) Torque curve

Figure 17. *Performance curves comparison.*

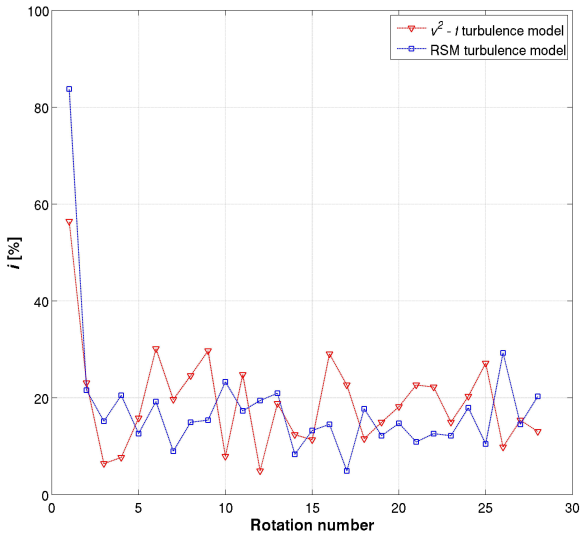

Figure 18. *Irregularity degree comparison for a conventional Savonius wind rotor with the conveyor–deflector curtain system.*

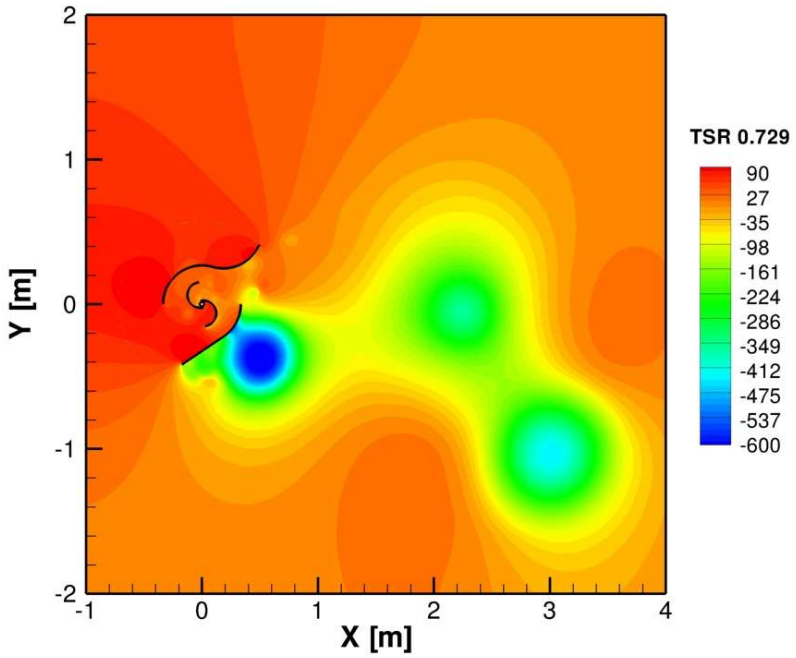

Figure 19. *Pressure contour [Pa] for a conventional Savonius wind rotor with the conveyor–deflector curtain system.*

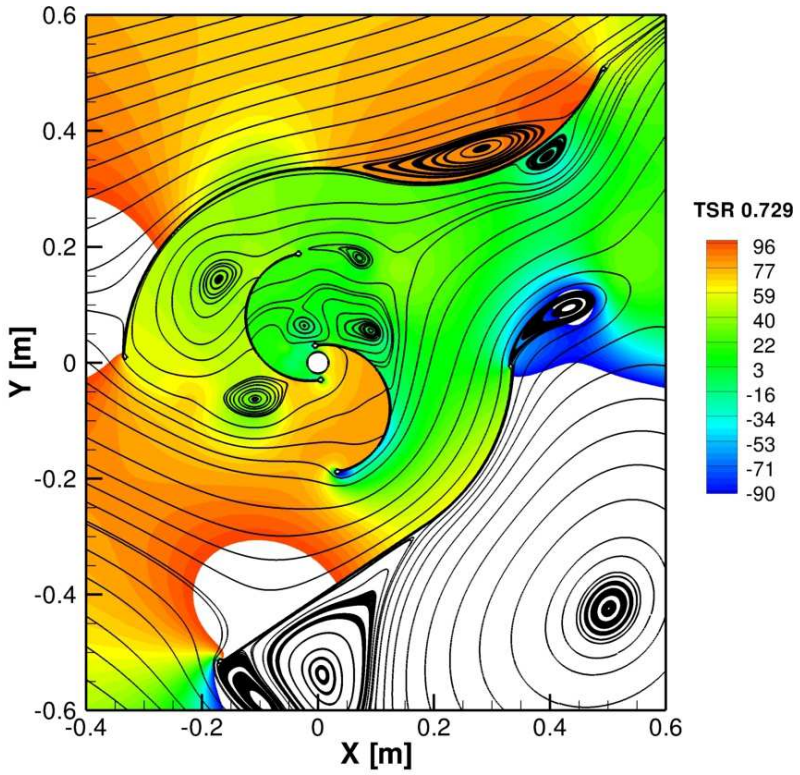

Figure 20. *Pressure contour [Pa] and streamlines of absolute velocity for a conventional Savonius wind rotor with the conveyor–deflector curtain system.*

References

[1] V.J. Modi and M.S.U.K. Fernando. On the performance of the Savonius wind turbine. In *7th WIND ENERGY SYMPOSIUM*. ASME, 1988.

[2] R. Ricci, S. Montelpare, G. Borrelli, and V. D'Alessandro. Experimental analysis of a Savonius wind rotor for streetlighting systems. In *Conference on Thermal and Environmental Issues in Energy Systems*. ASME–ATI–UIT, May 2010.

[3] R. Ricci, D. Vitali, and S. Montelpare. An innovative wind–solar hybrid street light: development and early testing of a prototype. *International Journal of Low–Carbon Technologies*, 2014.

[4] J.V. Akwa, H.A. Vielmo, and A.P. Petry. A review on the performance of Savonius wind turbines. *Renewable and Sustainable Energy Reviews*, 16:3054–3064, 2012.

[5] H.R. Rahai and H. Hefazi. Development of optimum design configuration and performance for vertical axis wind turbine. Feasibility Analysis and Final EISG (Energy Innovation Small Grant program) Report. Technical report, California Energy Commission, 2005.

[6] A.H. Benesh. The Benesh wind turbine. In *11th WIND ENERGY SYMPOSIUM*. ASME, 1992.

[7] M.A. Kamoji, S.B. Kedare, and S.V. Prabhu. Experimental investigations on single stage modified Savonius rotor. *Applied Energy*, 86:1064–1073, 2009.

[8] M.H. Mohamed, G. Janiga, Pap E., and Thévenin D. Optimal blade shape of a modified Savonius turbine using an obstacle shielding the returning blade. *Energy Conversion and Management*, 52:236–242, 2011.

[9] K. Kacprzak, G. Liskiewicz, and Sobczak K. Numerical investigation of conventional and modified Savonius wind turbines. *Renewable Energy*, 60:578–585, 2013.

[10] S. Roy and U.K. Saha. Review on the numerical investigations into the design and development of Savonius wind rotors. *Renewable and Sustainable Energy Reviews*, 24:73–83, 2013.

[11] K. Irabu and J.N. Roy. Characteristics of wind power on Savonius rotor using a guide–box tunnel. *Experimental Thermal and Fluid Science*, 32:580–586, 2007.

[12] B.D. Altan and M. Atilgan. The use of a curtain design to increase the performance level of a Savonius wind rotor. *Renewable Energy*, 35:821–829, 2010.

[13] M.H. Mohamed, G. Janiga, E. Pap, and D. Thévenin. Optimization of Savonius turbines using an obstacle shielding the returning blade. *Renewable Energy*, 35:2618–2626, 2010.

[14] K. Golecha, T.I. Eldho, and S.V. Prabhu. Influence of the deflector plate on the performance of modified Savonius water turbine. *Applied Energy*, 88:3207–3217, 2011.

[15] M.S.U.K. Fernando and V.J. Modi. A numerical analysis of the unsteady flow past a Savonius wind turbine. *Journal of Wind Engineering and Industrial Aerodynamics*, 32, 3:303–327, 1989.

[16] N. Fujisawa. Velocity measurements and numerical calculations of flow fields in and around Savonius rotors. *Journal of Wind Engineering and Industrial Aerodynamics*, 59:39–50, 1996.

[17] V. D'Alessandro, S. Montelpare, R. Ricci, and A. Secchiaroli. Unsteady Aerodynamics of a Savonius wind rotor: a new computational approach for the simulation of energy performance. *Energy*, 35:3349–3363, 2010.

[18] R. Ricci, S. Montelpare, A. Secchiaroli, and V. D'Alessandro. Flow field assessment in a vertical axis wind turbine. *WIT Transactions on Engineering Sciences*, 69:255–266, 2010.

[19] P. Jaohindy, H. Ennamiri, F. Garde, and A. Bastide. Numerical investigation of airflow through a Savonius rotor. *Wind Energy*, 2013.

[20] M. Selig. UIUC Applied Aerodynamics Group, Department of Aerospace Engineering, 2013. http://aerospace.illinois.edu/m-selig.

[21] F.R. Menter. Two–equation eddy–viscosity turbulence models for engineering applications. *AIAA Journal*, 32(8):1598–1605, 1994.

[22] F.R. Menter, R.B. Langtry, S.R. Likki, Y.B. Suzen, P.G. Huang, and S. Volker. A correlation-based transition model using local variables - Part 1: Model formulation. *Journal of Turbomachinery*, 128(3), 2006.

[23] F.R. Menter, R.B. Langtry, and S. Volker. Transition modelling for general purpose CFD codes. *Flow, Turbulence and Combustion*, 77, 2006.

[24] P.R. Spalart and S.R. Allmaras. A one-equation turbulent model for aerodynamic flows. *La Recherche Aérospatiale*, 1:5–21, 1994.

[25] P.A. Durbin. Near-wall turbulence closure modeling without "damping functions". *Theoretical and Computational Fluid Dynamics*, 3(1):1–13, 1991.

[26] V. Yakhot, S.A. Orszag, S. Thangam, T.B. Gatski, and C.G. Speziale. Development of turbulence models for shear flows by a double expansion technique. *Physics of Fluids A*, 4:1510–1520, 1992.

[27] M.M. Gibson and B.E. Launder. Ground effects on pressure fluctuations in the atmospheric boundary layer. *Journal of Fluid Mechanics*, 86:491–511, 1978.

[28] B. Launder and N Shima. Second–moment closure for the near-wall sublayer: development and application. *AIAA Journal*, 27:1319–1325, 1989.

[29] Ansys Inc., USA. *FLUENT User's guide, release 6.3.26*, 2006.

[30] J. Van Doormal and G. D. Raithby. Enhancement of the SIMPLE method for predicting incompressible flows. *Numerical Heat Transfer*, 7:147–163, 1984.